Applying a time-domain boundary element method for study of seismic ground response in the vicinity of embedded cylindrical cavity

H. Alielahi[1], M. Kamalian[2,*], J. Asgari Marnani[3], M. K. Jafari[4], M. Panji[1]

Abstract

In this paper, an advanced formulation of a time-domain two-dimensional boundary element method (BEM) is presented and applied to calculate the response of a buried, unlined, and infinitely long cylindrical cavity with a circular cross-section subjected to SV and P waves. The applicability and efficiency of the algorithm are verified with frequency-domain BEM examples of the effect of cylindrical cavities on the site response analysis. The analysis results show that acceptable agreements exist between results of this research and presented examples. For a shallow cavity, the numerical results demonstrate that vertically incident SV wave reduces the horizontal components of the motion on the ground surface above the cavity, while it significantly increases the vertical component for a dimensionless frequency (η) of 0.5 and h/a=1.5. The maximum values of normalized displacements in vertical component of P waves are larger than horizontal component of SV waves for η=1.0. For a deeply embedded cavity, the effect of the cavity on the surface ground motion is negligible for incident SV wave, but it increases the vertical component of the displacement for incident P wave. Additionally, far and near distances from the center of the cavity show different amplitude patterns of response due to the cavity effect. Increasing the distance from the center of the cavity, the amplitude of displacement and the effect of the cavity attenuates significantly.

Keywords: Boundary element method (BEM), Time-domain, Embedded cavity, Two-dimensional transient elastodynamic kernels, Scattering, Dynamic displacement.

1. Introduction

Scattering effects of an embedded cylindrical cavity on the ground surface waves are among the most interesting geotechnical earthquake engineering topics in recent years. Nowadays, subway tunnels in central urban areas are drastically implemented to improve the transportation quality and quantity. Construction of such large-scale cavities under the ground will certainly affect the ground motion and further

affect existing buildings nearby. Hence, it is important to estimate this effect on the seismic design of buildings. In this regard, different analytical and numerical studies have been published to date.

Numerical methods of the seismic study of the spatial ground response can be classified into two groups: domain type methods (e.g. finite element (FEM) and finite difference methods (FDM)) and boundary type methods (e.g. boundary element methods (BEM) and hybrid type methods). BEM, in comparison with FEM, only requires the discretization of the boundary of the domain interested and does not need any domain discretization. Additionally, BEM takes automatically Sommerfeld's radiation conditions at infinity for infinite and semi-infinite domains. Hence, this method does not need additional devices for treating problems such as stress concentrations [1].

BEM can be performed in two domains of time and frequency. Time-domain in comparison with frequency-domain boundary element methods, in that it provides a direct way of obtaining the time history of the response and it can be extended to the non-linear behavior. Bounded regions with

* *Corresponding Author: kamalian@iiees.ac.ir*
1 PhD Candidate, Department of Civil Engineering, Science and Research Branch, Islamic Azad University, Tehran, IRAN
2 Associate Professor, Department of Civil Engineering, Science and Research Branch, Islamic Azad University, Tehran, IRAN
3 Assistant Professor, Civil Engineering Department, Technical and Engineering Faculty, Central Tehran Branch, Islamic Azad University, Tehran, IRAN
4 Professor, Geotechnical Engineering Research Centre, International Institute of Earthquake Engineering and Seismology (IIEES), Tehran, IRAN

geometrical irregularity are modeled by the FEM, and the surrounding unbounded one is modeled by the BEM. Mansur [2] and Antes [3] were the firsts who formulated a time-stepping algorithm using two-dimensional kernels. But their traction kernels were very complicated, and appeared only implicitly in the BEM formulation. In this regard, Israil and Banerjee [4-6] introduced a new formulation which included simple and explicit kernels. While this formulation was easier to apply and could be used to evaluate the response of a structure either in a step-by-step time marching manner or by the superposition of the impulse response, a step-by-step marching scheme could be extended to non-linear cases [1]. Kamalian et al. [7-12] implemented modified kernels in site response analyses of topographic structures.

A review of published researches on the analytical and numerical 2-D evaluation of underground cylindrical cavity effects on the ground seismic response indicates that a majority of them were focused on analytical methods while introducing new methodologies. Pao and Mow [13] investigated the dynamic stress concentration of a single cavity in the whole space for incident elastic plane waves. Lee and Trifunac [14] studied the dynamic response of lined cylindrical cavities in a uniform elastic half-space to horizontal shear waves (*SH*) through Fourier-Bessel series expansion method. Crichlow [15] studied the two-dimensional finite element modeling of underground structural anomalies at shallow depths to obtain the response at the ground surface to damped, vertically incident, *SH*-waves. Dravinski [16] studied the scattering of plane harmonic horizontal shear waves (*SH*), vertical shear waves (*SV*), longitudinal waves (*P*) and Rayleigh waves by several inclusions of arbitrary shapes, completely embedded cavity within an elastic half-space. Lee and Karl [17] evaluated the scattering and diffraction of plane *SV* waves by underground, circular, cylindrical cavities at various depths in an elastic half-space. They used Fourier-Bessel series in analytical method. Using an indirect boundary integral method based on two-dimensional Green functions for a visco-elastic half-space, De Barros and Luco [18] studied the response of a viscoelastic half-space containing a buried, unlined, infinitely long cylindrical cavity with circular cross-section subjected to harmonic plane *SH, P, SV* and Rayleigh waves. Manoogian and Lee [19] applied the weighted residual method to the problem of scattering and diffraction of plane *SH*-waves by an underground cavity of different elastic mediums with arbitrary shape in a two-dimensional half-space. Later, Manoogian [20] applied the same method for the problem of the scattering and diffraction of plane elastic waves, in the form of *SH* waves, by a tunnel of arbitrary shape located below the surface of a two-dimensional half-space. Davis et al. [21] investigated the transverse response of underground cylindrical cavities and pipes to incident *SV* waves. They implemented analytical solutions for unlined cavities embedded within an elastic half-space by using Fourier Bessel series and a convex approximation of the half-space free surface. Jianwel and Lee [22, 23] performed a series of solutions for surface motion amplification due to underground twin cavities for incident plane *P* and *SV* waves derived by Fourier-Bessel series expansion method. Rodriguez-Castellanos et al. [24] verified the effect of the

indirect boundary element method on 2D scattering of elastic P and SV waves. Geometries considered in this study were planar and elliptic cracks and cavities. Smerzini et al. [25] used expansions of wave functions in terms of Bessel and Hankel functions for studying the anti-plane seismic response of underground structures subjected to the incidence of both plane and cylindrical waves. They assumed that the structure was a circular inclusion embedded in a homogenous, isotropic and linear visco-elastic half-space. Yu and Dravinski [26] reported anti-plane-strain model for the steady-state scattering of elastic waves by a rough inclusion or a cavity embedded in a half- space by using a direct boundary integral equation method for a plane harmonic SH wave. Yu and Dravinski [27] investigated the scattering of plane harmonic *P, SV* or Rayleigh waves through a direct boundary integral equation method by a 2-D smooth and rough cavity completely embedded in an isotropic half-space and full-space. Yu and Dravinski [28] evaluated the scattering of a plane harmonic *P, SV* or Rayleigh wave by a corrugated elastic inclusion completely embedded in a two-dimensional isotropic half-space and full space using a direct boundary integral equation method.

As mentioned above, almost all BEM applications to the study of the cavity's effect on the seismic site response reported in the literature were restricted to the frequency-domain. The important limitation of the analysis in frequency-domain is its shortcoming in non-linear problems. This paper applies an advanced time-domain BEM in order to execute the ground site response underlain by unlined cavities that are subjected to vertically propagating *SV* and *P* incident waves. The applicability and efficiency of the presented algorithm is demonstrated by analyzing the response of a buried, unlined and infinitely long cylindrical cavity with a circular cross-section subjected to *SV* and *P* waves.

2. Formulation of the Problem

The governing equation for an elastic, isotropic and homogeneous body with a small amplitude displacement field can be written as:

$$\left(c_1^2 - c_2^2\right) \cdot u_{j,ij}(x,t) + c_2^2 \cdot u_{i,jj}(x,t) + b_i(x,t) - \ddot{u}_i(x,t) = 0 \qquad (1)$$

in which u_i denotes the displacement vector, b_i indicates the body force vector, and c_1 and c_2 are the spreading velocities of the compressional and shear waves respectively, where $c_1^2 = (\lambda + 2\mu)/\rho$ and $c_2^2 = \mu/\rho$, in which, λ and μ are the Lame constants and ρ is the mass density. In this paper, soil behavior is assumed to be linear and the body forces are neglected.

In cases where the domain Γ contains holes, contours are more than one. In another word, a finite number of non-intersecting inner contours are enclosed by an outer boundary. This type of domain, in mathematical terms, is referred to as a multiplied connected domain [29, 30]. The geometry of the model is illustrated in Fig. 1.

Using the well-known weighted residual method, the governing boundary integral equation for the elastic, isotropic, and homogeneous half-plane domain Γ containing holes and ignoring contributions from initial conditions and body forces can be written as:

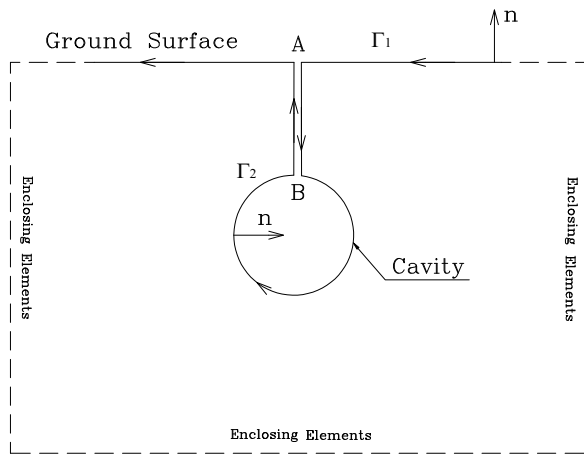*H. Alielahi, M. Kamalian, J. Asgari Marnani, M. K. Jafari, M. Panji*

Fig. 1 Schematic geometry of a multiplied connected domain by BEM. The integral direction is Counterclockwise on the ground surface and Clockwise on the cavity

$$c_{ij}(\xi) \cdot u_i(\xi,t) = \int_{\Gamma_1} \left(G_{ij}(x,\xi,t) \otimes t_i(x,t) - F_{ij}(x,\xi,t) \otimes u_i(x,t) \right) \cdot d\Gamma \quad (2)$$
$$+ \int_{\Gamma_2} \left(G_{ij}(x,\xi,t) \otimes t_i(x,t) - F_{ij}(x,\xi,t) \otimes u_i(x,t) \right) \cdot d\Gamma$$
$$+ \int_{AB} \left(G_{ij}(x,\xi,t) \otimes t_i(x,t) - F_{ij}(x,\xi,t) \otimes u_i(x,t) \right) \cdot d\Gamma$$
$$+ \int_{BA} \left(G_{ij}(x,\xi,t) \otimes t_i(x,t) - F_{ij}(x,\xi,t) \otimes u_i(x,t) \right) \cdot d\Gamma$$

Also it is noted that:

$$\int_{AB} \left(G_{ij}(x,\xi,t) \otimes t_i(x,t) - F_{ij}(x,\xi,t) \otimes u_i(x,t) \right) \cdot d\Gamma = \quad (3)$$
$$- \int_{BA} \left(G_{ij}(x,\xi,t) \otimes t_i(x,t) - F_{ij}(x,\xi,t) \otimes u_i(x,t) \right) \cdot d\Gamma$$

and
$$\Gamma = \Gamma_1 + \Gamma_2$$

Thus:

$$c_{ij}(\xi) \cdot u_i(\xi,t) = \int_{\Gamma_1} \left(G_{ij}(x,\xi,t) \otimes t_i(x,t) - F_{ij}(x,\xi,t) \otimes u_i(x,t) \right) \cdot d\Gamma$$
$$+ \int_{\Gamma_2} \left(G_{ij}(x,\xi,t) \otimes t_i(x,t) - F_{ij}(x,\xi,t) \otimes u_i(x,t) \right) \cdot d\Gamma$$
$$= \int_{\Gamma} \left(G_{ij}(x,\xi,t) \otimes t_i(x,t) - F_{ij}(x,\xi,t) \otimes u_i(x,t) \right) \cdot d\Gamma \quad (4)$$

For seismic loading, assuming that the total displacement can be split into incident ($u_j^{inc.}$) and scattered ($u_i^{sc.}$) components, the governing boundary integral equation (BIE) should be modified as follow [7, 9, 10, 11]:

$$c_{ij}(\xi) \cdot u_i(\xi,t) = \int_{\Gamma} \left(G_{ij}(x,\xi,t) \otimes t_i(x,t) - F_{ij}(x,\xi,t) \otimes u_i(x,t) \right) \cdot d\Gamma + u_j^{inc.}(\xi,t) \quad (5)$$

G_{ij} and F_{ij}, are the transient displacement and traction fundamental solutions of Eq.1, respectively, and denote the i th components of displacements and tractions at a point x at time t, due to a unit point force applied in direction j at point ξ at the preceding time τ. $G_{ij} \otimes t_i$ and $F_{ij} \otimes u_i$ denote the Riemann-convolution integrals, the operation $\otimes$ denotes time convolution like:

$$f \otimes g = \int_0^t f(x,t-\tau) g(x,\tau) d\tau$$

where "f" and "g" are two functions and "t" is the time. This operation is applied in order to simplify the governing boundary equations and c_{ij} is the well-known discontinuity term resulting from the singularity of the traction fundamental solution kernel. Implementation of boundary integral Eq.2, needs approximation in both temporal and spatial variations of field variables. For temporal integration, the time axis from 0 to T is divided into N equal steps of duration Δt, i.e. $T=N\Delta t$.

2.1. Numerical Discretization

Eq.1 is an exact representation of the transient problem of the seismic response of a homogenous isotropic substructure cavity, since no approximation has yet been introduced. However, for the practical problem, suitable approximations are needed for both the spatial and temporal variations of field variables. As will be shown, temporal integrations of the time functions involved will be performed analytically, whereas the spatial integration should be performed using numerical techniques.

Linear time variation
Using a linear time variation of field variables, displacements and tractions are expressed as:

$$u_i(x,\tau) = M_1(\tau) \cdot u_i^n(x) + M_2(\tau) \cdot u_i^{n-1}(x) \quad (6)$$

$$t_i(x,\tau) = M_1(\tau) \cdot t_i^n(x) + M_2(\tau) \cdot t_i^{n-1}(x)$$

where $M_1(\tau)$ and $M_2(\tau)$ are linear temporal shape functions given by:

$$(n-1)\Delta t \prec \tau \prec n\Delta t :$$
$$M_1(\tau) = \frac{\tau - T_{n-1}}{\Delta t} \quad \& \quad M_2(\tau) = \frac{T_n - \tau}{\Delta t} \quad (7)$$

Subscripts 1 and 2 refer to the forward and backward temporal nodes during a time step, respectively. Thus the time integration involves only kernels and is expressed by:

$$G_{ij1}^{N+1-n}(r) = \int_{(n-1)\Delta t}^{n \cdot \Delta t} G_{ij}(r,t-\tau) \cdot M_1(\tau) \cdot d\tau \quad (8)$$

$$G_{ij2}^{N+1-n}(r) = \int_{(n-1)\Delta t}^{n \cdot \Delta t} G_{ij}(r,t-\tau) \cdot M_2(\tau) \cdot d\tau$$

Where G_{ij1}^{N+1-n} and G_{ij2}^{N+1-n} are the time-convoluted elastodynamic traction kernels for the forward and backward time nodes during a time step, respectively, which are derived analytically [7].

Temporal integration
For temporal integration, the time axis is divided into N equal steps i.e. $T=N\Delta t$. Combining this and a similar expression for the F-kernels in Eq.5, after spatial discretization and some rearrangements, the convoluted BEM equation for linear temporal variation can be written as:

$$c_{ij} \cdot u_i^N(\xi) = \sum_{n=1}^{N} \sum_{q=1}^{Q} \left\{ T_{ik}^n \cdot \int_{\Gamma_q} G_{ij}^{N+1-n}(r) \cdot L_k \cdot d\Gamma_q - U_{ik}^n \cdot \int_{\Gamma_q} F_{ij}^{N+1-n}(r) \cdot L_k \cdot d\Gamma_q \right\} + u_j^{inc.}(\xi,t) \quad (9)$$

In which:

$$G_{ij}^{N+1-n}(r) = G_{ij1}^{N+1-n}(r) + G_{ij2}^{N-n}(r) \qquad (10)$$

$$F_{ij}^{N+1-n}(r) = F_{ij1}^{N+1-n}(r) + F_{ij2}^{N-n}(r)$$

N indicates the last time step, Q shows the total number of boundary elements and L represents the interpolation function of a boundary element. G_{ij}^{N+1-n} and F_{ij}^{N+1-n} are the elasto-dynamic displacement and traction kernels, respectively, derived from their corresponding fundamental solutions F_{ij} and G_{ij}, as presented before [7].

The assembled system of equation takes the following matrix form by sequentially writing Eq.9 for each boundary node at the time of $t+\Delta t$ and by transferring all known terms to the right side:

$$F^I.U^N = G^I.T^N + Z^N \qquad (11)$$

In which:

$$Z^N = \sum_{n=1}^{N-1}\left(G^{N+1-n} \cdot T^n - F^{N+1-n} \cdot U^n\right) + U^{inc.N} \qquad (12)$$

U^N and T^N denote the nodal displacement and traction vectors at the current time node, respectively. Z^N includes both effects of the past dynamic history and the incident motion on the current time node.

It should be mentioned that the spatial integral of Eqs.11 and 12 could be performed easily using the Gaussian normal quadrature rule, provided an intelligent sub-segmentation with suitable mapping is adopted to make the kernel-shape function-Jacobian product well behaved over each sub-segment. Strongly singular blocks in F^1 could be evaluated indirectly using the concept of the rigid body motion [31]. This technique is valid only for problems with closed boundaries and the unbounded boundaries of half-plane problems which should be enclosed with fictitious ones.

3. Numerical Verifications and Discussions

The above-mentioned formulation has been implemented in a computer code named SAMBE (Seismic Analysis of Multiple Boundary Element). The numerical examples presented in this section demonstrate the applicability and efficiency of the proposed time-stepping BEM in order to carry out the response of an embedded, unlined, infinitely long cylindrical cavity with a circular cross-section subjected to incident SV and P waves. The embedded cavity was subjected to vertically propagating incident waves of the Ricker type (Fig. 2):

$$f(t) = A_{max} \cdot \left[1 - 2 \cdot (\pi \cdot f_p \cdot (t-t_0))^2\right] e^{-(\pi \cdot f_p \cdot (t-t_0))^2} \qquad (13)$$

where f_p, t_0, and A_{max} denote the predominant frequency, time shift parameter, and maximum amplitude of the time history, respectively.

3.1. Verification of the Results with De Barros and Luco [18]

The purpose of the present verification is to illustrate the applicability and accuracy of the presented BE algorithm in calculating dynamic displacements in the vicinity of an embedded cylindrical cavity in a linear elastic half-plane. The
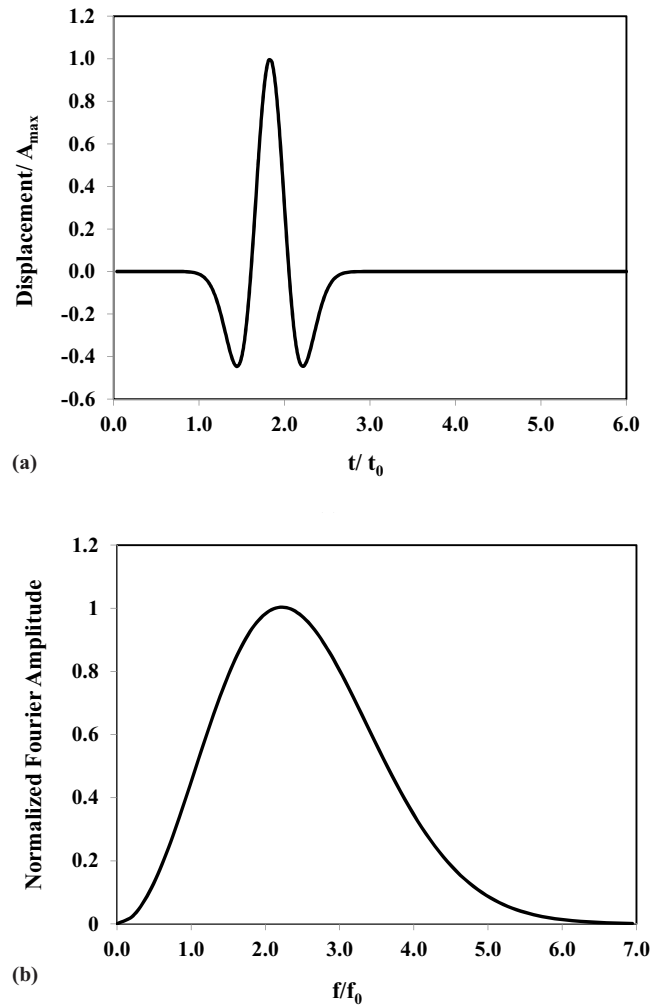

Fig. 2 (a) Displacement time history and (b) Fourier amplitude of the Ricker wave type

problem presented in this section is studied in a dimensionless form by De Barros and Luco [18] for weakly inelastic media. Fig. 3 shows the geometry used for embedded cylindrical cavity analysis in a homogeneous half-plane subjected to vertically propagating incident SV and P waves of the Ricker type. In this figure, "h" is the depth of the cavity center-line below the free surface and "a" is the radius of the cavity.

The Ricker wave has a predominant frequency of 1.5 Hz, time shift parameter of 0.675 sec and maximum amplitude of 0.001 m. The cavity has a radius of 50 m. The shear wave velocity, Poisson's ratio and mass density are 223.33 m/s, 0.33 and 2.0 ton/m³, respectively. In order to discretize the problem, 245 quadratic boundary elements were used. Five different time steps of 0.015, 0.020, 0.025, 0.035, and 0.05 have been chosen, combinations of which with element size give proper values of 0.025 and 10 m for time steps and cavity element size, respectively.

3.1.1. The Results of SV Incident Waves

Figs. 4 to 7 illustrate the comparison of the normalized amplitude of total horizontal and vertical displacement on the ground surface and cavity wall. This normalization has been done by De Barros and Luco [18] through the amplitude of
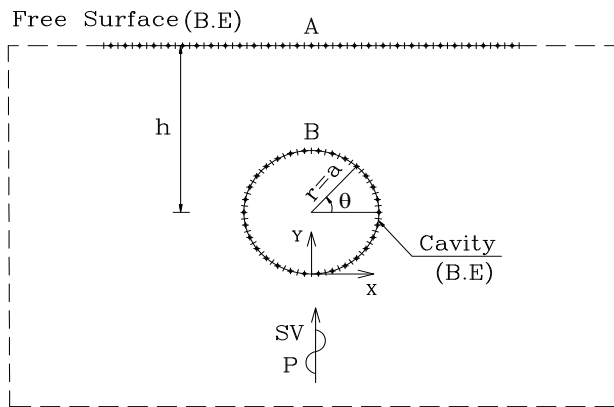
H. Alielahi, M. Kamalian, J. Asgari Marnani, M. K. Jafari, M. Panji

Fig. 3 Schematic geometry and discretization of the embedded cylindrical cavity subjected to vertically propagating incident SV and P waves of the Ricker type
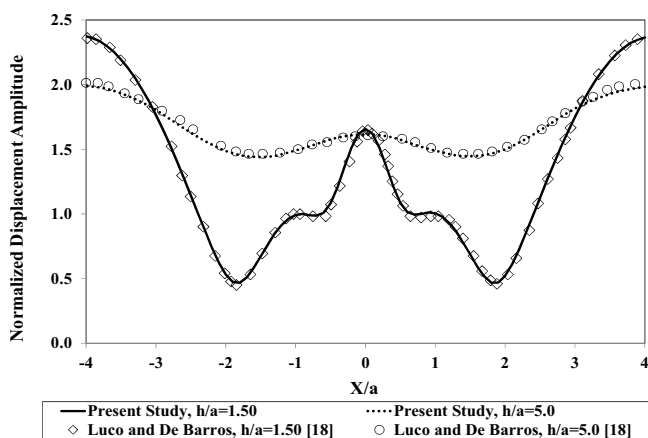
vertical *SV* incident waves on the ground surface. Results for h/a=1.5 and 5.0 are shown for normalized frequency (η=ωa/πc$_2$) of 0.5, where ω: presents the angular frequency of the wave, and "a" and "c$_2$": denote the radius of the cavity and shear wave velocity of medium, respectively. The dimensionless frequency defined as the ratio of twice the radius of the cavity to the shear wavelength. Results of horizontal and vertical displacement components are different from free-field motion. As it is observed, acceptable results are obtained by the BE method in purely elastic medium for incident *SV* waves, whereas, De Barros and Luco (1994) results include a small amount of attenuation. The main target of Luco and De Barros (1994) studies are validating two-dimensional viscoelastic green's functions by indirect boundary integral method with previous studies in purely elastic medium. Hence, in order to resolve previous study
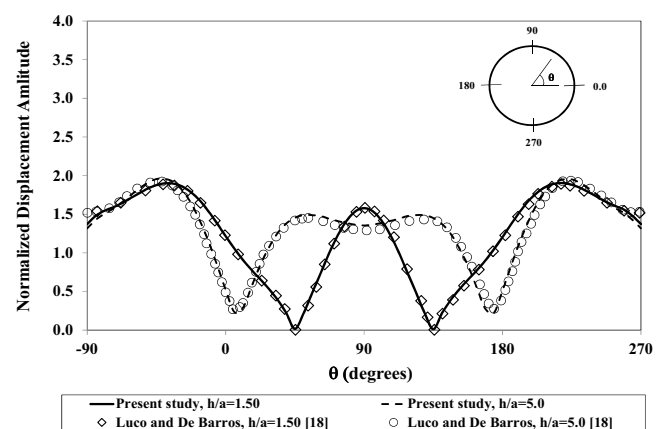

Fig. 4 Normalized amplitude of total horizontal displacement on the ground surface due to embedded cylindrical cavity in case of the vertically incident SV waves and η=0.5. The solid and dashed lines represent the horizontal component of displacement for shallow (h/a=1.5) and deep (h/a=5.0) cavity obtained by BE method, respectively. The diamond and circle symbols represent the horizontal component of displacement for shallow and deep cavity obtained by Luco and De Barros [18], respectively
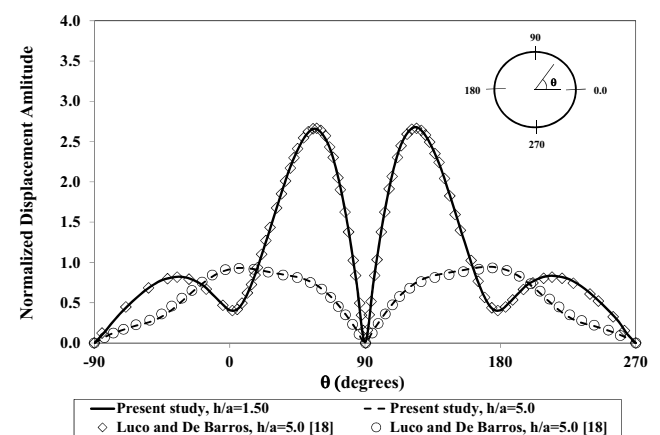

Fig. 6 Normalized amplitude of total horizontal displacement on the cylindrical cavity wall in case of the vertically incident SV waves and η=0.5. The solid and dashed lines represent the horizontal component of displacement for shallow (h/a=1.5) and deep (h/a=5.0) cavity obtained by BE method, respectively. The diamond and circle symbols represent the horizontal component of displacement for shallow and deep cavity obtained by Luco and De Barros [18], respectively

Fig. 5 Normalized amplitude of total vertical displacement on the ground surface due to embedded cylindrical cavity in case of the vertically incident *SV* waves and η=0.5. The solid and dashed lines represent the vertical component of displacement for shallow (h/a=1.5) and deep (h/a=5.0) cavity obtained by BE method, respectively. The diamond and circle symbols represent the vertical component of displacement for shallow and deep cavity obtained by Luco and De Barros [18], respectively

Fig. 7 Normalized amplitude of total vertical displacement on the cylindrical cavity wall in case of the vertically incident SV waves and η=0.5. The solid and dashed lines represent the vertical component of displacement for shallow (h/a=1.5) and deep (h/a=5.0) cavity obtained by BE method, respectively. The diamond and circle symbols represent the vertical component of displacement for shallow and deep cavity obtained by Luco and De Barros [18], respectively

problems with viscoelastic green's functions, a small amount of damping (nonzero) was needed to be considered by Luco and De Barros (1994).

Figs. 8 and 9 compare the ground responses obtained at points A and B via different time steps in case of the incident SV waves. As it is seen, suitable agreements exist between results obtained by the BE method via different time steps. Results for horizontal and vertical components are quite different. For vertically incident SV waves, the presence of a shallow cavity (h/a=1.50) in comparison with free-field motion reduces horizontal components of motion on the ground surface above the cavity for a dimensionless frequency (η) of 0.5, whereas it increases vertical components significantly. Additionally, for a deeply embedded cavity (h/a=5.0), the effect of the cavity on the surface ground motion is small for η=0.5. Figs. 6 and 7 show normalized amplitudes of the total displacement on the cavity wall for four points on the cavity wall (θ = 0, 90, 180 and 270˚). In a shallow cavity (h/a=1.5), the vertical component of displacement on the cavity wall for SV waves is greater than its horizontal component for η=0.5.
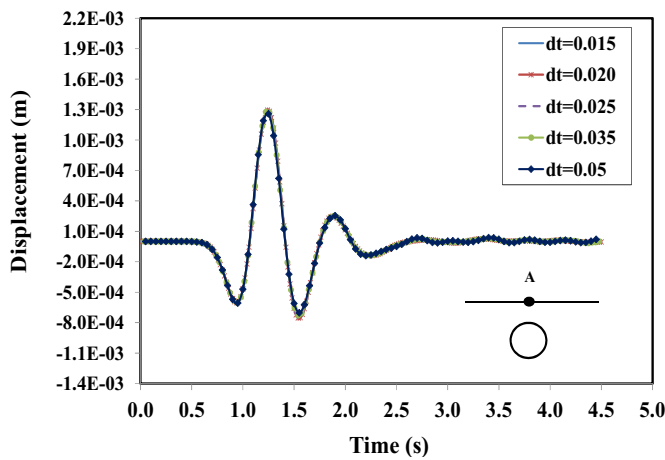
3.1.2. The Results of P Incident Waves

In this section of the study, the results of BEM code are compared with De Barros and Luco's [18] studies for *P* incident waves. The comparison of normalized amplitude of total horizontal and vertical displacements on the ground surface and cavity wall are respectively demonstrated on Figs. 10 to 13. As it is observed, acceptable results are obtained by the BE method for incident *P* waves. The ground responses obtained at points A and B via different time steps in case of the incident *P* waves are demonstrated on Figs. 14 and 15. As it is seen, proper agreements exist between results by the BE method via different time steps. *SV* waves have different responses compared to the results of *P* waves. The presence of a shallow cavity (h/a=1.50) in comparison with free-field motion, for vertically incident *P* waves

Fig. 8 Horizontal displacement time histories at point (A) via different time steps, in the case of vertically propagating incident *SV* waves
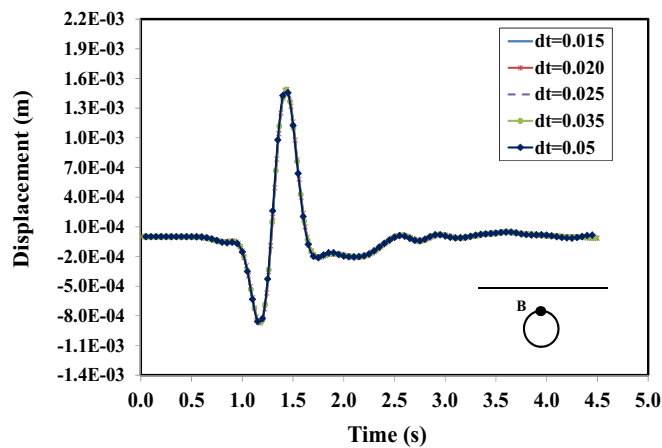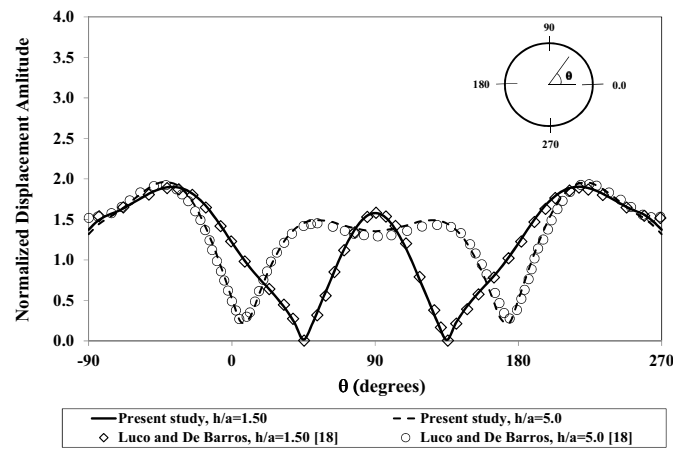
Fig. 10 Normalized amplitude of total horizontal displacement on the ground surface due to embedded cylindrical cavity in case of the vertically incident P waves and η=0.5. The solid and dashed lines represent the horizontal component of displacement for shallow (h/a=1.5) and deep (h/a=5.0) cavity obtained by BE method, respectively. The diamond and circle symbols represent the horizontal component of displacement for shallow and deep cavity obtained by Luco and De Barros [18], respectively
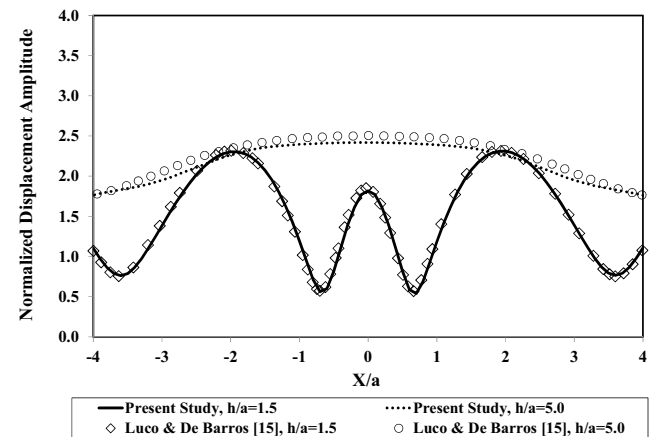
Fig. 9 Horizontal displacement time histories at point (B) via different time steps in case of vertically propagating incident *SV* waves

Fig. 11 Normalized amplitude of total vertical displacement on the ground surface due to embedded cylindrical cavity in case of the vertically incident P waves and η=0.5. The solid and dashed lines represent the vertical component of displacement for shallow (h/a=1.5) and deep (h/a=5.0) cavity obtained by BE method, respectively. The diamond and circle symbols represent the vertical component of displacement for shallow and deep cavity obtained by Luco and De Barros [18], respectively

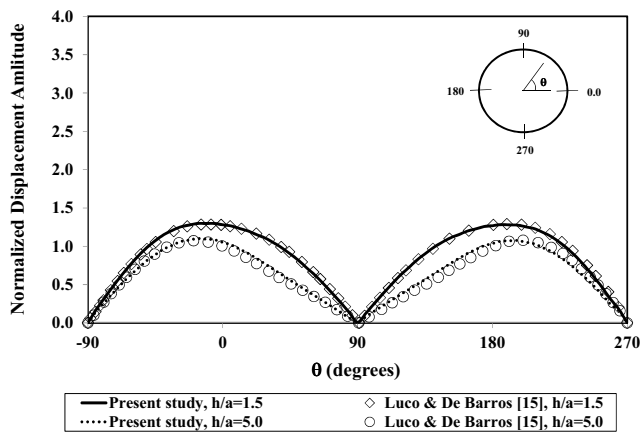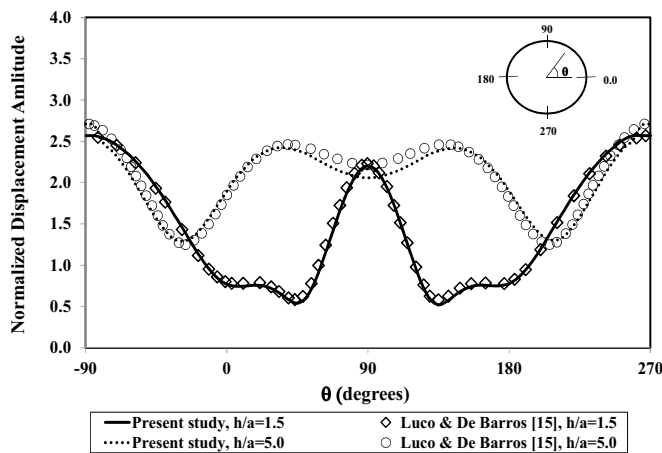*H. Alielahi, M. Kamalian, J. Asgari Marnani, M. K. Jafari, M. Panji*

Fig. 12 Normalized amplitude of total horizontal displacement on the cylindrical cavity wall in case of the vertically incident P waves and η=0.5. The solid and dashed lines represent the horizontal component of displacement for shallow (h/a=1.5) and deep (h/a=5.0) cavity obtained by BE method, respectively. The diamond and circle symbols represent the horizontal component of displacement for shallow and deep cavity obtained by Luco and De Barros [18], respectively

Fig. 13 Normalized amplitude of total vertical displacement on the cylindrical cavity wall in case of the vertically incident P waves and η=0.5. The solid and dashed lines represent the vertical component of displacement for shallow (h/a=1.5) and deep (h/a=5.0) cavity obtained by BE method, respectively. The diamond and circle symbols represent the vertical component of displacement for shallow and deep cavity obtained by Luco and De Barros [18], respectively
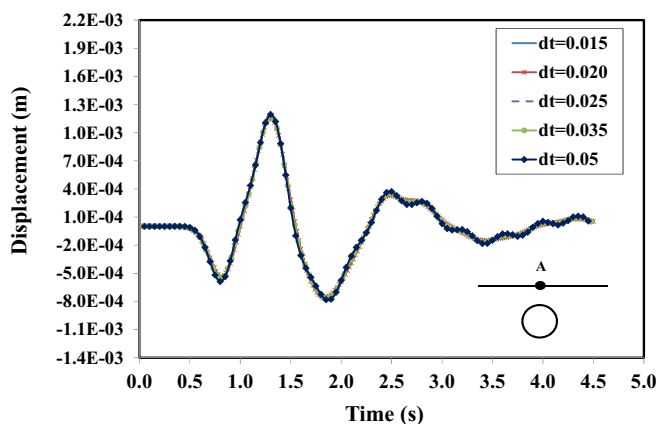
increases vertical components of motion on the ground surface above the cavity for η=0.5, whereas it reduces horizontal components. The effect of the cavity on horizontal components of surface ground motion is small for a deeply embedded cavity (h/a=5.0), however, for vertical components are vice versa at η=0.5. Normalized amplitudes of the total displacement for four points on the cavity wall (θ = 0, 90, 180 and 270˚) are shown on Figs. 12 and 13. The vertical component of displacement on the cavity wall for *P* waves is greater than its horizontal component in shallow cavity (h/a=1.5) for a dimensionless frequency (η) of 0.5.

3.2. Verification of the Results with Yu and Dravinski [27]

The aim of this verification is to show the accuracy and applicability of the presented BE algorithm in order to investigate the scattering pattern by smooth cavity which is completely embedded in a linear elastic half-space subjected to vertically propagating incident *SV* and *P* waves of the Ricker type (Fig. 3). The problem descript in this section is in a dimensionless form investigated by Yu and Dravinski [27]. The mass density and shear wave velocity of the half-plane are chosen to be 2.0 ton/m³ and 223.33 m/s, respectively. The cavity has a radius of 50 m. The Poisson's ratio of the material is chosen to be 0.33. The predominant frequency, the time shift parameter and the maximum amplitude of the incident motion are chosen as 3.0 Hz, 0.675 sec and 0.001 m, respectively. The problem is solved by using a BE method with 245 quadratic elements.

3.2.1. The Results of SV Incident Waves
The normalized horizontal and vertical displacement amplitude of a half-space medium subjected to the incident motions with those obtained by Yu and Dravinski [27] are compared and shown on Figs. 16 and 17 for a dimensionless frequency (η) of 1.0 and h/a=2.0. This study suggests that appropriate results are obtained by the BE method for incident *SV* waves. Figs. 18 and 19 compare the ground response obtained at points A and B via different time steps in case of incident *SV* waves. As illustrated, suitable agreements are observed between results obtained by the BE method via
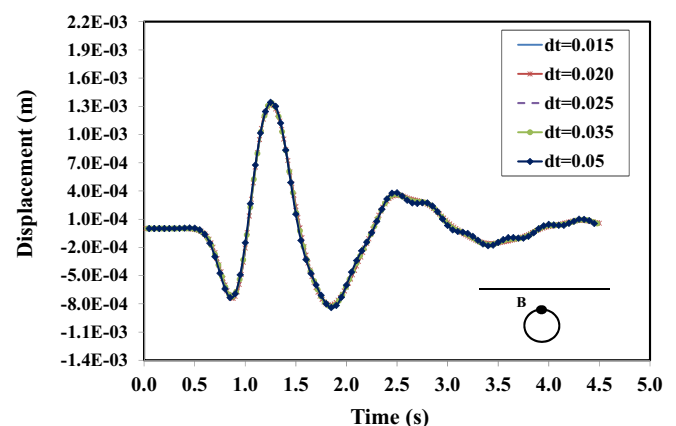

Fig. 14 Vertical displacement time histories at point (A) via different time steps in case of vertically propagating incident P waves

Fig. 15 Vertical displacement time histories at point (B) via different time steps in case of vertically propagating incident P waves
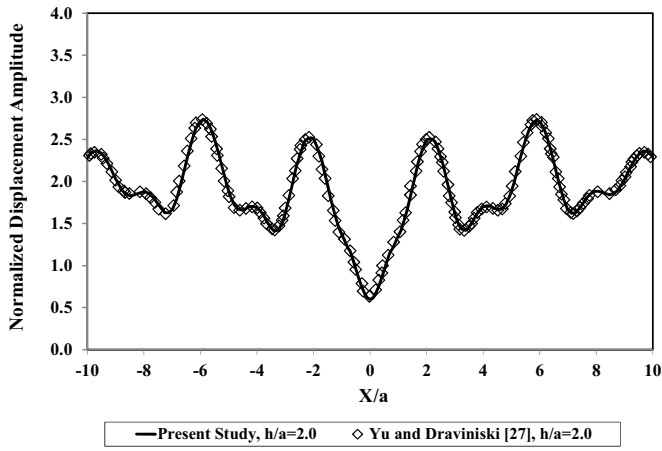
Fig. 16 Normalized amplitude of total horizontal displacement on the ground surface due to embedded smooth cavity in case of the vertically incident SV waves and η=1.0. The solid line represent the horizontal component of displacement for h/a=2.0 obtained by BE method. The diamond symbols represent the horizontal component of displacement for h/a=2.0 obtained by Yu and Draviniski [27], respectively
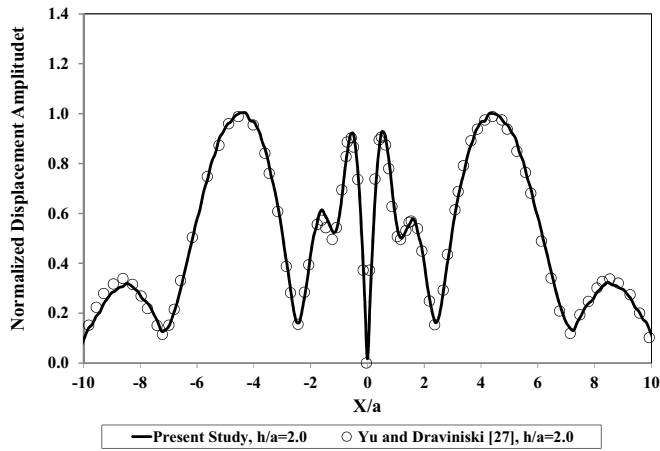

Fig. 17 Normalized amplitude of total vertical displacement on the ground surface due to embedded smooth cavity in case of the vertically incident SV waves and η=1.0. The solid line represent the vertical component of displacement for h/a=2.0 obtained by BE method. The circle symbols represent the vertical component of displacement for h/a=2.0 obtained by Yu and Draviniski [27], respectively
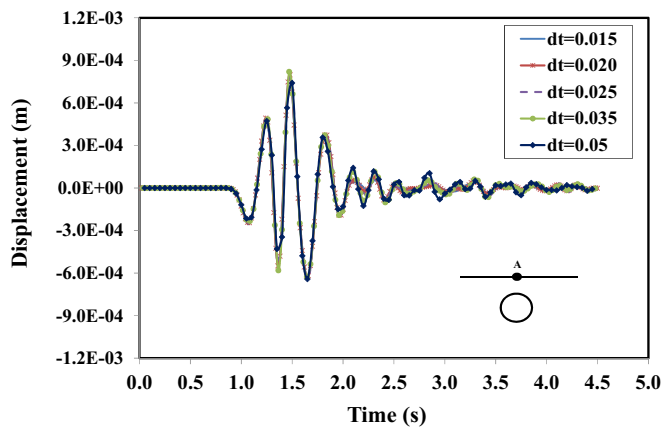

Fig. 18 Horizontal displacement time histories at point (A) via different time steps in case of vertically propagating incident *SV* waves
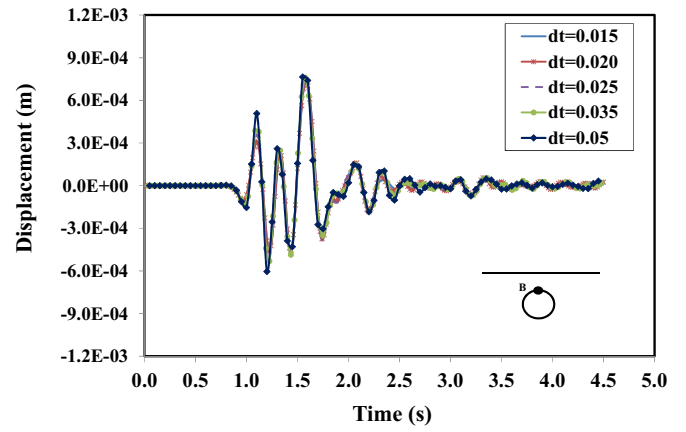

Fig. 19 Horizontal displacement time histories at point (B) via different time steps in case of vertically propagating incident SV waves

different time steps. Results of horizontal and vertical displacement components are different from free-field motion. For a vertically incident *SV* wave, the half-space surface motion can be divided into two groups including │X│>5a and│X│≤5a. According to Figs. 16 and 17, it can be observed that amplitude of displacements attenuates in the case of │X│>5a in comparison with│X│≤5a.

3.2.2. The Results of P Incident Waves

Figs. 20 and 21 for a dimensionless frequency of 1.0 and h/a=2.0 provide comparison between the normalized horizontal and vertical displacement amplitude of a half-space medium subjected to the incident *P* waves with those obtained by Yu and Dravinski [27]. The ground response obtained at points A and B via different time steps are demonstrated on Figs. 22 and 23 in case of incident *P* waves. Suitable agreements are observed between results by the BE method as illustrated via different time steps. As it is observed, the maximum values of normalized displacements in vertical component of *P* waves are larger than horizontal component of *SV* waves for η=1.0. It is also noticeable in comparison of *SV* vertical component with
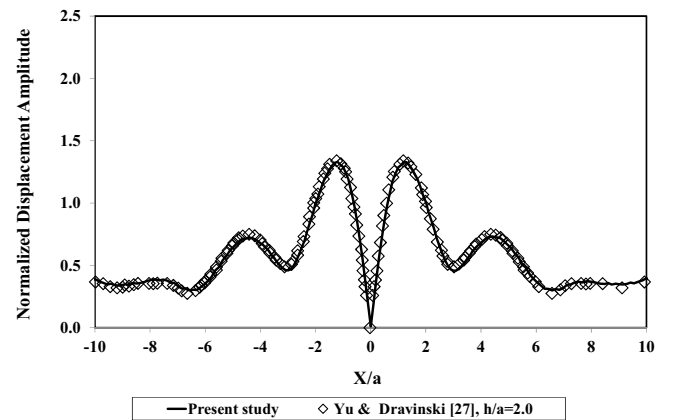

Fig. 20 Normalized amplitude of total horizontal displacement on the ground surface due to embedded smooth cavity in case of the vertically incident P waves and η=1.0. The solid line represent the horizontal component of displacement for h/a=2.0 obtained by BE method. The diamond symbols represent the horizontal component of displacement for h/a=2.0 obtained by Yu and Draviniski [27], respectively

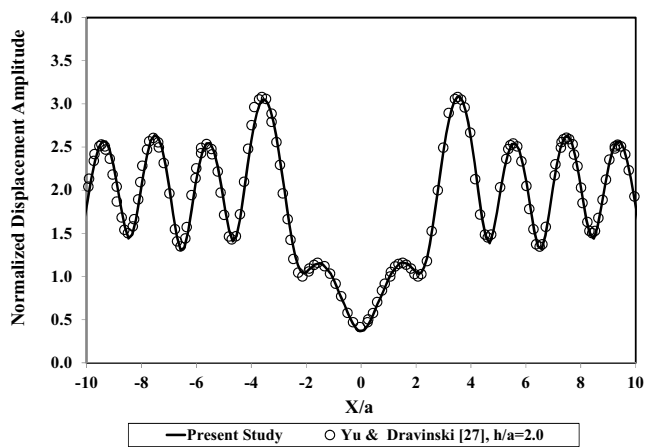*H. Alielahi, M. Kamalian, J. Asgari Marnani, M. K. Jafari, M. Panji*

Fig. 21 Normalized amplitude of total vertical displacement on the ground surface due to embedded smooth cavity in case of the vertically incident P waves and η=1.0. The solid line represent the vertical component of displacement for h/a=2.0 obtained by BE method. The circle symbols represent the vertical component of displacement for h/a=2.0 obtained by Yu and Draviniski [27], respectively
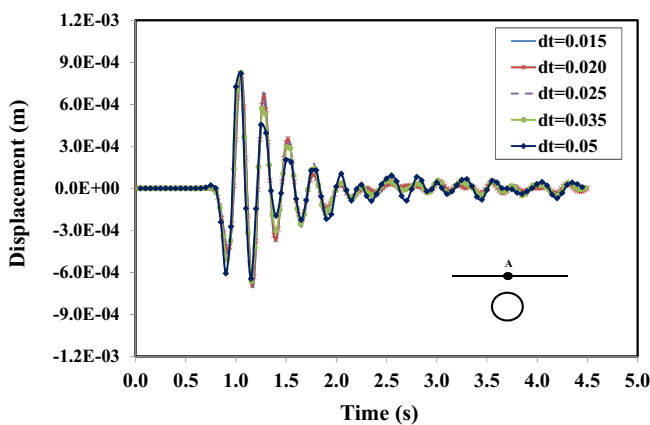

Fig. 22 Vertical displacement time histories at point (A) via different time steps in case of vertically propagating incident P waves

horizontal component of *P* waves. The half-space surface motion can be divided into two groups including │X│ ›5a and │X│ ≤5a for a horizontally incident *P* waves. It could be observed that amplitude of displacements attenuates in the case of │X│ ›5a according to Figs. 20 and 21.

4. Conclusion

In this paper, an advanced time stepping BEM algorithm is presented and applied to attain the response of an embedded, unlined and infinitely long cylindrical cavity with a circular cross-section subjected to *SV* and *P* waves in time-domain.

The applicability and efficiency of the algorithm have been demonstrated by comparing the results of the present research with those of frequency-domain BEM examples concerning the effect of cylindrical cavity on the site response analysis. The compared examples were an embedded cylindrical cavity studied by De Barros and Luco [18] and an embedded smooth unlined cavity subjected to vertical incident *SV* and *P* waves investigated by Yu and Dravinski [27]. Since the presented algorithm is completely formulated in time-domain, it enables the extension
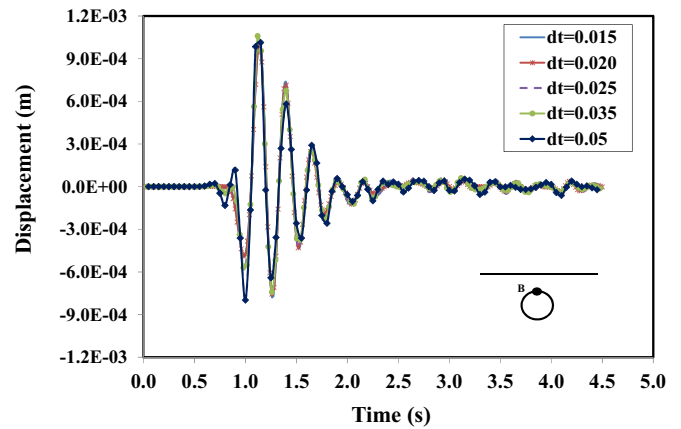

Fig. 23 Vertical displacement time histories at point (B) via different time steps in case of vertically propagating incident P waves

of solving scattering problems and calculating dynamic displacements of two-dimensional cavity structures with non-linear behavior. Numerical results show that for a vertically incident *SV* wave, a shallow cavity in comparison with free-field motion reduces the horizontal component of the motion on the ground surface above the cavity, while it significantly increases the vertical component for η=0.5. However, for a *P* wave, the vertical of displacement is increased compared to displacements of those of the horizontal component for η=0.5. For a deeply embedded cavity, the effect of the cavity on the surface ground motion is negligible for incident *SV* wave, but in case of *P* wave the vertical component of displacement is increased. As it is observed, the maximum values of normalized displacements in vertical component of *P* waves are larger than horizontal component of *SV* waves for η=1.0. It is also noticeable in comparison of *SV* vertical component with horizontal component of *P* waves. Additionally, far and near distances from the center of the cavity show different amplitude patterns of response displacement. The effect of the cavity on ground surface for the far distance response amplitude is observed to be smaller than that of near distance motion. At last it should be mentioned that in this research the effect of the underground cavities on the seismic ground response was investigated using the time domain BEM. Of course this type of problems can be solved using other numerical methods including the finite element method (FEM) [32] as well as the discrete element method (DEM) [33, 34] and all obtained results deserve to be compared in the future.

Refrences

[1] Beskos, D.E.:1987, Boundary Element Methods in Dynamic Analysis, Appl. Mech. Rev., 40(1), 1-23.

[2] Mansur WJ.:1983, A Time-stepping Technique to Solve Wave Propagation Problems Using the Boundary Element Method, Ph.D. Dissertation, Southampton University.

[3] Antes H.:1985, A Boundary Element Procedure for Transient Wave Propagation in Two-dimensional Isotropic Elastic Media, Journal of Finite Elem. Anal. and Des., 1, 313-322.

[4] Israil ASM, Banerjee PK.:1990, Advanced Time Domain Formulation of BEM for Two-dimensional Transient Elastodynamics, Int. Journal for Numerical Methods in Eng., 29, 1421-1440.

[5] Israil ASM, Banerjee PK.:1990, Two- dimensional Transient Wave Propagation by Time Domain BEM, Int. Journal of. Solids and Structures, 26, 851-864.

[6] Israil ASM, Banerjee PK.:1992, Advanced Development of Boundary Element Method for Two-dimensional Dynamic Elasto-plasticity, Int. Journal of Solids and Structures, 29, 1433-1451.

[7] Kamalian, M., Gatmiri, B., Sohrabi-Bidar, A.: 2003a, On Time-Domain Two-Dimensional Site Response Analysis of Topographic Structures by BEM, Journal of Seismology and Earthquake Engineering, 5, 35-45.

[8] Kamalian, M., Jafari, M. K., Dehghan, K., Sohrabi-Bidar, A., Razmkhah, A.: 2003b, Two- Dimensional Hybrid Response Analysis of Trapezoidal Shaped Hills In Time Domain, Advances in Boundary Element Techniques IV, Ed. Gallego R and Aliabadi MH, pp. 231-236.

[9] Kamalian, M., Sohrabi-Bidar, A.: 2006, Transient Site Response Analysis of Nonhomogeneous Two-dimensional Topographic Features Using BEM, Esteghlal, Journal of Engineering. Isfahan University of Technology. (in Persian)

[10] Kamalian, M., Gatmiri, B., Sohrabi-Bidar, A. and Khalaj, A.: 2007a, Amplification Pattern of 2D Semi-sine Shaped Valleys Subjected to Vertically Propagating Incident Waves, Commun. Numer. Methods Eng., 23, 871– 887.

[11] Kamalian, M., Jafari, M.K., Sohrabi-Bidar, A. and Razmkhah, A.: 2008a, Seismic Response of 2D Semi-sine Shaped Hills to Vertically Propagating Incident Waves: Amplification Patterns and Engineering Applications, Earthq. Spectra, 24(2), 405–430.

[12] Kamalian, M., Sohrabi-Bidar, A., Razmkhah, A., Taghavi, A. and Rahmani, I.: 2008b, Considerations on Seismic Microzonation in Areas with Two-dimensional Hills, J. Earth Syst. Sci., 117, 783–796.

[13] Pow YH, Mow CC.:1973, Diffraction of Elastic Waves and Dynamic Stress Concentrations. Rand Corp., Crane Russak and Co. Publishers Inc: New York.

[14] Lee, V. W., Trifunac, M. D.:1979, Response of Tunnels to Incident SH Waves, J. Eng. Mech. Div., Am. Soc. Civ. Eng., 105(4), 643–659.

[15] Crichlow, Joel M.:1982, The Effect of Underground Structure on Seismic Motions of the Ground Surface, Geophys. J. R. astr. SOC, 70, 563-575.

[16] Dravinski, M.: 1983, Ground Motion Amplification due to Elastic Inclusions in a Half-space, Journal of Earthquake Engineering and Structural Dynamics, 11, 313-335.

[17] Lee, V. W., Karl, J.:1992, Diffraction of SV Waves by Underground, Circular, Cylindrical Cavities, Journal of Soil Dynamics and Earthquake Engineering, 11, 445-456.

[18] Luco, JE, De Barros, FCP.:1994, Dynamic Displacements and Stresses in the Vicinity of a Cylindrical Cavity Embedded in a Half-space, Earthquake Engineering and Structural Dynamics, 23, 321-340.

[19] Manoogian, M. E. and Lee,V. W.:1996, Diffraction of SH-Waves by Subsurface Inclusions of Arbitrary Shape, Journal of Engineering Mechanics, 122(2), 123-129.

[20] Manoogian, M. E.:2000, Scattering and Diffraction of SH Waves Above an Arbitrarily Shaped Tunnel, SET Journal of Earthquake Technology, 37(399), 11-26.

[21] Davis, C. A., Lee, V. W. and Bardet, J. P.: 2001, Transverse Response of Underground Cavities and Pipes to Incident SV Waves, Earthquake Engineering and Structural Dynamics, 30, 383-410.

[22] Jianwel, Liang., Hao, Zhang., Lee, Vincent W.: 2003, A Series Solution for Surface Motion Amplification Due to Underground Twin Tunnels Incident SV Waves, Earthquake Engineering and Engineering Vibration, 2(2), 289-298.

[23] Jianwel, Liang., Hao, Zhang., Lee, Vincent W.: 2004, A Series Solution for Surface Motion Amplification due to Underground Group Cavities: Incident P Waves, Acta Seismologica Sinica, 17(3), 296-307.

[24] Rodriguez-Castellanos, A., Sanchez-Sesma, F. J. Luzon, F. and Martin R.: 2006, Multiple Scattering of Elastic Waves by Subsurface Fractures and Cavities, Bulletin of the Seismological Society of America, 96(4A), 1359–1374.

[25] Smerzini, C., Aviles, J., Sanchez-Sesma, F. J and R. Paolucci.: 2009, Effect of Underground Cavities on Surface Earthquake Ground Motion under SH Wave Propagation, Earthquake Engineering and Structural Dynamics. 32(12), 1441-1460.

[26] Yu, C.W., Dravinski, M.: 2009, Scattering of Plane Harmonic SH Wave by a Completely Embedded Corrugated Scatterer, Int. J. Num. Meth. Engng. 78, 196–214.

[27] Yu, C.W., Dravinski, M.: 2009, Scattering of Plane Harmonic P, SV and Rayleigh Waves by a Completely Embedded Corrugated Cavity, Geophys J Int. 178, 479–487.

[28] Yu, C.W., Dravinski, M.: 2010, Scattering of Plane Harmonic P, SV and Rayleigh Waves by a Completely Corrugated elastic inclusion, Wave Motion. 47, 156–167.

[29] Katsikadelis, J.T.: 2002, Boundary Elements: Theory and Applications, Elsevier Science Ltd.

[30] Brebbia, CA., Dominguez, J.:1989, Boundary Elements, an Introductory Course, Southampton: Computational Mechanics Publication.

[31] Ahmad, S., and Banerjee, P. K.: 1988, Multi-domain BEM for Two-dimensional Problems of Elastodynamics, Int. J. Numer. Methods Eng. 26, 891–911.

[32] Miraboutalebi, M., Askari, F., Farzaneh, O.: 2011, Effect of Bedrock Inclination on Seismic Slope Stability according to Iran Seismically Data, International Journal of Civil Engineering, Vol. 9, No. 4. pp. 247-254.

[33] Shahnazari, H., Esmaeli, M., Hossini Rangbar, H.: 2010, Simulating the Effects of Projectile Explosion on a Jointed Rock Mass Using 2D DEM: A Case Study of Ardebil-Mianeh Railway Tunnel, International Journal of Civil Engineering, Vol. 8, No. 1. pp. 125-133.

[34] Majidi, A. R. , Mirghasemi, A. A., Arabshahi, M.: 2011, Three Dimensional Bearing Capacity Analysis of Shallow Foundations using Discrete Element Method, International Journal of Civil Engineering, Vol. 9, No. 4. pp. 282-292.